SMAR 2019 – Fifth Conference on Smart Monitoring,
Assessment and Rehabilitation of Civil Structures

Structural evaluation of a reactor building during pressure leak-rate testing for life extension assessment

Marcelo A. CEBALLOS [1,2], Carlos F. ESTRADA [1], Federico PINTO [1,2], Marcelo POMERANTZ[3], Carlos A. PRATO [1,*]

[1] Universidad Nacional de Córdoba, Córdoba, Argentina

[2] Consejo Nacional de Investigaciones Científicas y Técnicas, Argentina

[3] Nucleoeléctrica Argentina (NA-SA), Argentina

[*] Contact e-mail: prato_carlos@yahoo.com

ABSTRACT: As a part of a life extension project, a pressure leak-rate test has been carried out at the Embalse NPP, located in Córdoba (Argentina). Testing consisted of applying a differential pressure of 126 kPa inside the reactor building in order to represent the design basis accident. Both leakage rate and structural deformations were monitored at several locations of the pre-stressed containment structure in order to evaluate its response with respect to model predictions considering linear elastic response. Given the fact that the testing was performed over several days, when significant thermal fluctuations took place, both internal and external temperatures were recorded before, during, and after the testing. The thermal records were then introduced in a numerical model to evaluate the resulting deformations that were expected to be of the same order as those due to the internal pressure. This paper describes the pressure leak-rate test, the instrumentation used and the results, with particular emphasis on the modeling procedure to account for the rather complex thermal variations that took place during the test, that were to be filtered out in order to assess the response of the building due to the applied pressure.

1 INTRODUCTION

A general layout of the pre-stressed concrete containment structure (CS) of the Embalse NPP is shown in Figure 1. It consists on a cylindrical shell capped with a spherical dome, supported by a base slab that also serves as foundation for the reinforced concrete internal structure (IS). The cylindrical part is provided with four buttresses that increase its stiffness and connect the base slab with a massive ring beam connecting the cylinder with the roof dome. The plant was designed and built in the 1970's, and had begun to operate in 1984.

After 30 years of continuous service, the NPP underwent a general overhaul of its functional components and instrumentation. A number of structural assessments of the civil structures have also been carried out over the last 12 years, such as its capacity to sustain upgraded seismic demands based on actual seismic records and enhanced numerical evaluations (Pinto et al., 2007; Ceballos et al., 2007). As the last step of that process, a pressure leak-rate test was carried out. This test was performed during the month of December 2018, and as corresponds to the climate at the location of the plant (30º latitude) at the start of the summer season, considerable daily and seasonal thermal changes of the structure took place in parallel to the pressurization program.

In addition to displacements and strains of the CS, particular attention was given to recording the temperature oscillations induced by radiation and air temperature changes that were expected to

occur in phase with the stress-induced deformations associated with the increase of internal pressure. Deformations induced by thermal effects tend to obscure those caused by the internal pressure, and have to be filtered out from those due to the pressure to assess the measured response with numerical model results. For that purpose, special attention was given to the instrumentation to record temperature changes at both internal and external surfaces of the concrete structure. The temperature changes across the thickness of the concrete components was not instrumented but were obtained through simulations performed with the numerical model.

Temperature records of nodes at both the internal and external surfaces of the CS walls were fed into the finite element model (FEM); the temperature at internal points across the thickness was computed until they reached a quasi-steady state condition. Such approach required to measure temperatures for two weeks' time before the initiation of the pressure tests, and for one additional week after the pressurization had finished. This simulation of the temperature effects within the mass of concrete provided an estimate of thermally induced changes to be deducted from the displacements recorded during the pressure leak-rate test.

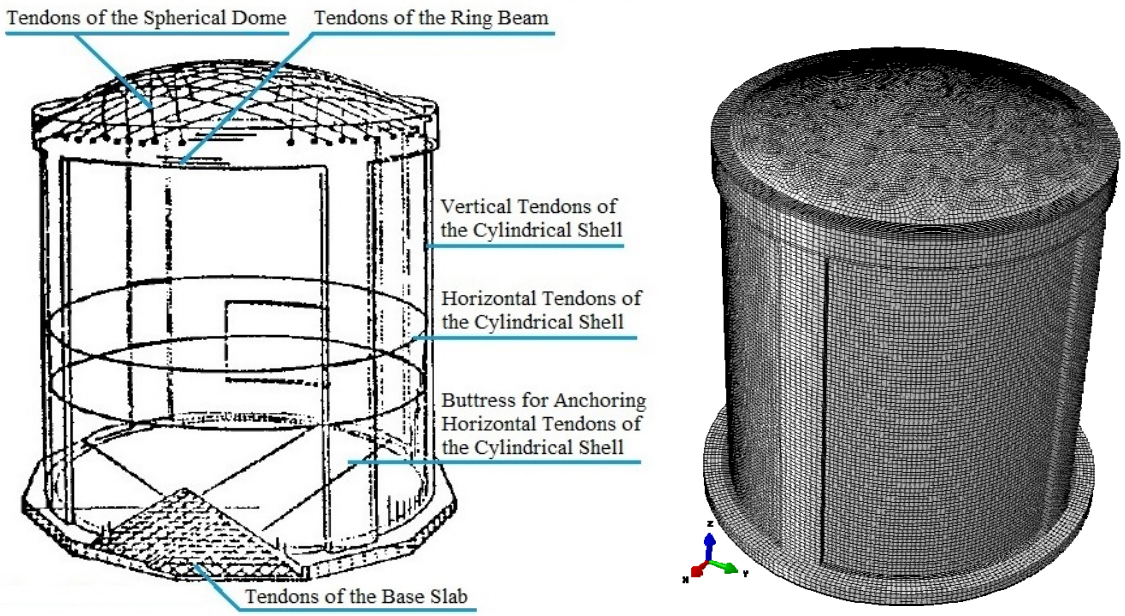

Figure 1. General layout of the CS of the Embalse NPP (left) and a view of the numerical model (right).

2 INSTRUMENTATION

Three types of instruments were installed on the CS for the test: surface temperature transducers, displacement transducers on the internal surface and strain transducers at internal surface points. The positioning of the various types of instruments is indicated in Figure 2.

2.1 Surface temperature transducers

The transducers used to record temperatures are of two types: thermographic cameras for the exterior surface, and contact sensors for both the interior surface and the outer surface area with permanent shadow produced by the proximity to the Service Building (thick line in the left of Figure 2, that cover the lower half in height). Figure 3 shows two typical images acquired by thermographic cameras, which have a resolution of 120 pixels in height by 160 pixels in width (with a total of 19200 pixels). In these images the geometry of the CS can clearly be appreciated,

where light tones indicate high temperatures while dark tones involve low temperatures or areas that do not belong to the surface of the CS. The images were subdivided for the analysis in macro-pixels of 10x10 pixels in order to obtain average values of each sector of the outer surface. A detailed analysis of these macro-pixels allowed to establish that the temperature is practically constant in height for each instant and in each meridian of the cylindrical shell, so such hypothesis was adopted for the numerical model.

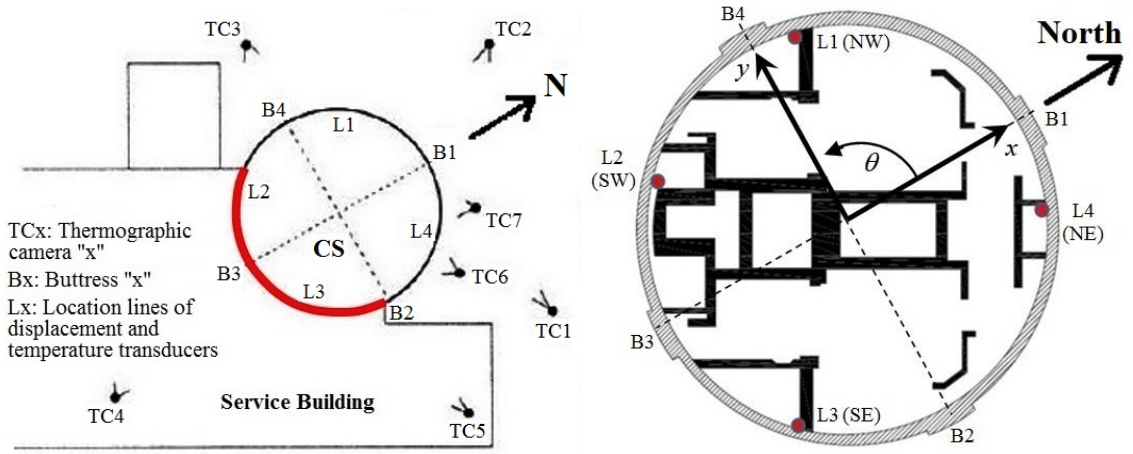

Figure 2. Position of thermographic cameras outside (left) and transducer location lines inside CS (right).

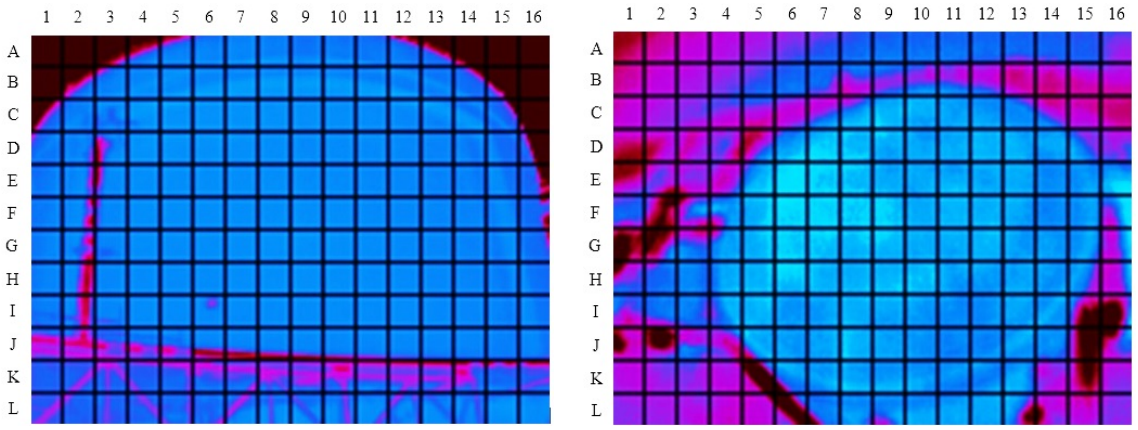

Figure 3. Images obtained with thermographic cameras TC1 (left) and TC5 taking the dome (right).

For the circumferential coordinate, the temperatures are defined analytically for each instant by adjusting the following terms of the Fourier series with the least squares criterion:

$$T(\theta) = A_0 + A_1 \cos(\theta) + B_1 \sin(\theta) + A_2 \cos(2\theta) + B_2 \sin(2\theta) \quad (1)$$

The angle θ is defined in the counter clockwise from the direction pointing north, as indicated in Figure 2. The temperature on the outer surface of the dome is defined constant by quadrants: NW, SW, SE, and NE. In the permanent shadow area near the Service Building, the temperature is defined constant for each instant, calculated as the average of the records taken there.

Figure 4 shows a comparison of external and internal temperatures near the dome apex, together with the evolution of the internal pressure during the leak-rate test.

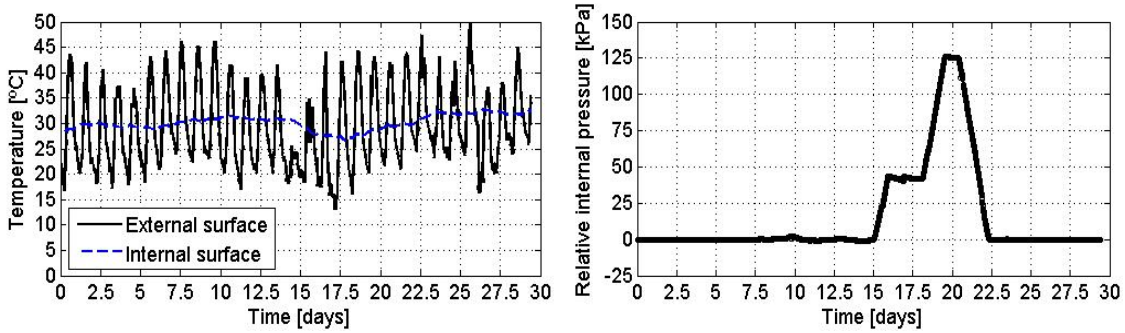

Figure 4. Comparison of external and internal temperatures near the dome apex (left) and evolution of internal pressure during the leak-rate test (right).

2.2 Displacement transducers on the internal surface

The displacement transducers used are of LVDT-type, and were placed at different heights on lines L1, L2, L3 and L4 indicated in Figure 2. One of them was placed in the vertical direction near the dome apex. The designation and location of the 19 LVDT transducers are indicated in Table 1, together with the contact thermometers at the same locations.

2.3 Strain transducers at internal surface points

The 6 strain gauge transducers used were placed as follows: 2 on line L2, 2 on line L4, and 2 in perpendicular directions at a point near the dome apex. The location and designation of these transducers and its corresponding contact thermometers are also given in Table 1.

Table 1. Designation and location of transducers on the Containment Structure

Dome			Line L1			Line L2			Line L3			Line L4		
Displacement transducers														
Temp. trans.	Disp. trans.	Elev. [m]	Temp. trans.	Disp. trans.	Elev. [m]	Temp. trans.	Disp. trans.	Elev. [m]	Temp. trans.	Disp. trans.	Elev. [m]	Temp. trans.	Disp. trans.	Elev. [m]
TI01	**MD01**	145.1	TI11	MD11	100.0	TI21	MD21	98.2	TI31	MD31	100.0	TI41	MD41	101.8
			TI12	MD12	106.7	TI22	MD22	105.4	TI32	MD32	106.7	TI42	MD42	108.3
			TI13	MD13	112.5	TI23	MD23	112.5	TI33	MD33	112.5	TI43	MD43	113.9
			TI14	MD14	117.4	TI24	**MD24**	120.5	TI34	MD34	117.4	TI44	MD44	119.9
						TI25	MD25	128.1				TI45	MD45	128.8
Strain gauges														
Temp. trans.	Strain trans.	Elev. [m]	Temp. trans.	Strain trans.	Elev. [m]	Temp. trans.	Strain trans.	Elev. [m]	Temp. trans.	Strain trans.	Elev. [m]	Temp. trans.	Strain trans.	Elev. [m]
TI02	SG01	145.1				TI22	SG22	105.9				TI42	SG42	108.8
TI02	SG02	145.1				TI23	SG23	113.0				TI43	SG43	114.0

3 RESULTS

In order to assess the results of the pressure leak-rate test, a numerical model was developed in the ABAQUS program (2010), whose thermo-mechanical parameters were adjusted to achieve an optimal correspondence between the measured and calculated behaviors. The details of the calibration process are presented elsewhere by Ceballos et al. (2019). Figure 1 shows on the right a view of this numerical model.

Figure 5 shows the time variation of the computed temperature across the thickness at point MD24 located on the cylindrical shell and at point MD01 near the dome apex. The continuous lines refer to computed variations of temperature as a function of time in different points across the wall thickness, starting the simulation on "day 0.00", while the dotted lines represent the resulting temperature variations when the simulation starts on "day 0.50".

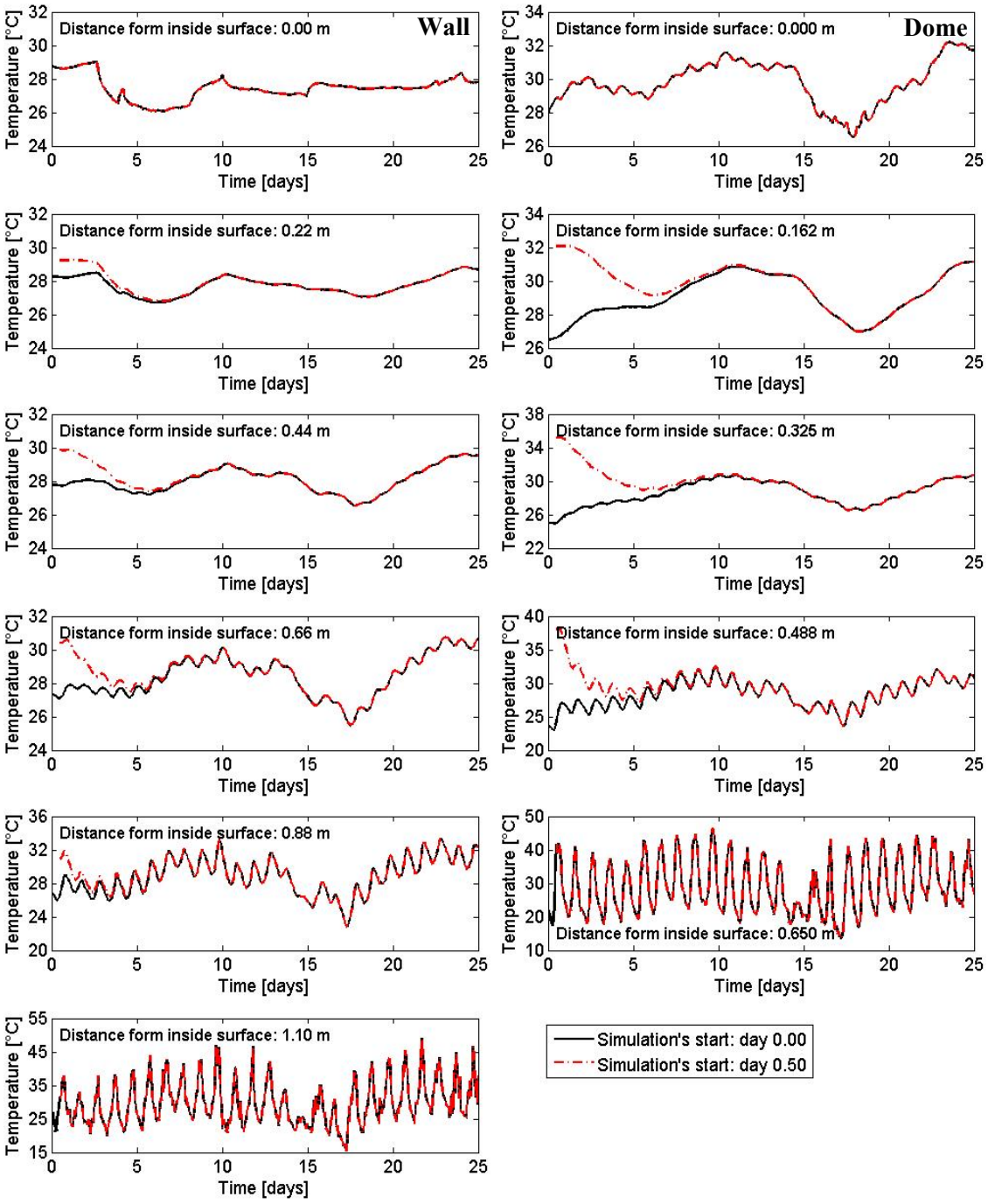

Figure 5. Computed time variation of the temperature across the thickness at point MD24 on the cylindrical shell (left) and at point MD01 near the dome apex (right).

These two sets of computed temperatures as function of time, show the largest differences in the first days, and converge to each other at about day 10. The temperatures from this moment are then taken as the initial values for all nodes to calculate the temperature-induced displacements during the pressure leak-rate test. It is observed that the curves of both the inner surface (distance of 0.00 m from inside surface) and the outer surface (distance of 1.10 m for the wall, and 0.65 m for the dome) are independent of the instant chosen for the beginning of the simulation, since these temperatures are imposed in the numerical model.

Figure 6 shows a comparison of the temperature distribution across the thickness at point MD24 on the wall (with a thickness of 1.10 m) and at point MD01 near the center of the dome (with a thickness of 0.65 m). These results show that temperature distributions across the thickness at day 10.50 are independent of the initial temperature assumed for the internal nodes. It is noted that the temperature distribution for day 0.50, starting on the same instant, initially shows a linear variation. It can also be seen that for days 5.50 and 10.50, the computed temperature variation across the thickness is far from linear and independent of the initial conditions assumed for the internal nodes. The resulting temperature distribution for nodes at day 10.50 is then adopted as the initial temperature for all nodes in order to calculate the displacements caused only by the measured temperatures of the internal and external surfaces of the CS in the period of time when the internal pressure is applied.

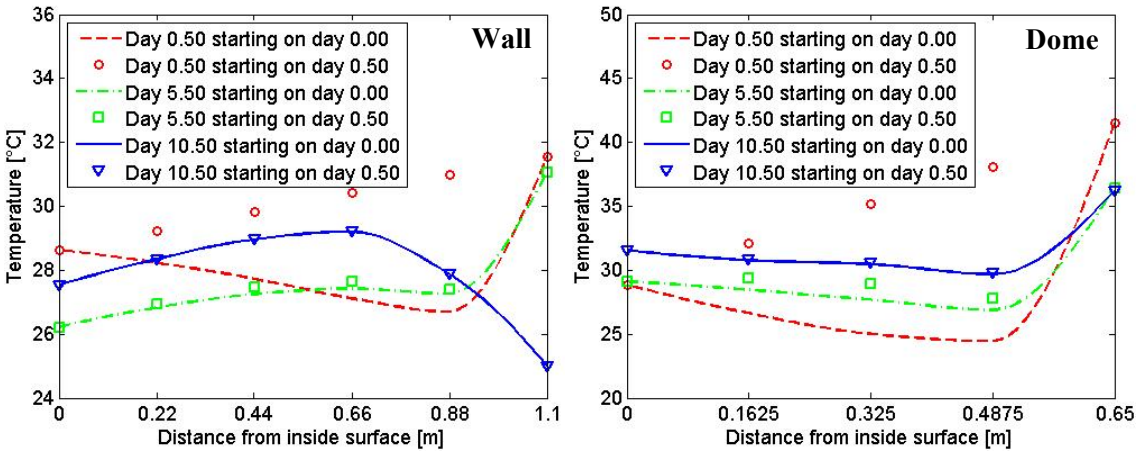

Figure 6. Evolution in time of the temperature distribution across the thickness at point MD24 on the wall (left) and at point MD01 near the dome apex (right) obtained from the numerical simulation.

Figure 7 shows a comparison of normal displacements given by: i) Measured displacement records, ii) Computed displacements obtained by means of the numerical model due to combined temperature and pressure changes, and iii) Computed displacements obtained with the numerical model due only to internal pressure. It seems of interest to point out that the temperature effects on the displacements at the dome are not significant, whereas for point MD24 on the cylindrical wall it is noted that the maximum measured displacement is close to 3 mm. At the same point, the corresponding computed maximum displacement due only to pressure is approximately 2 mm. In other words, the thermal induced maximum displacements turn out to be approximately 50% of those induced by pressure.

Figure 8 shows a comparison of computed normal displacements due to internal pressure with those of smoothened measured displacements, where computed thermal effects evaluated by the numerical model have been filtered out. The largest difference between these two sets is found to be for the maximum displacement at the dome, which was observed to be 8 mm, whereas the model yields 10 mm.

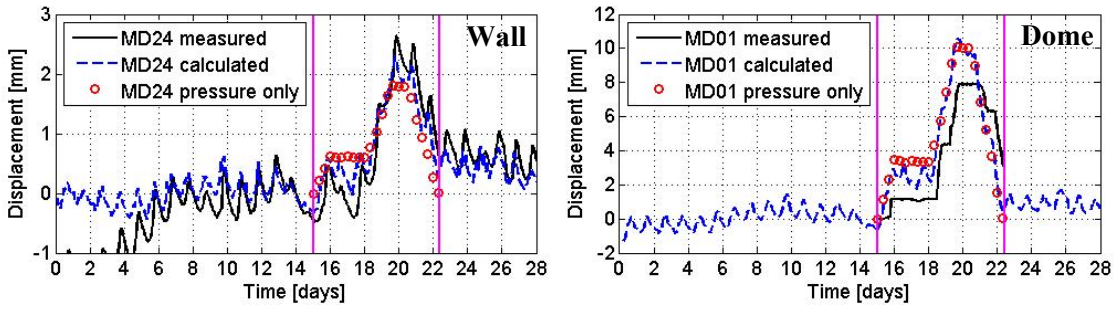

Figure 7. Total displacements caused by combined changes of pressure and temperature.

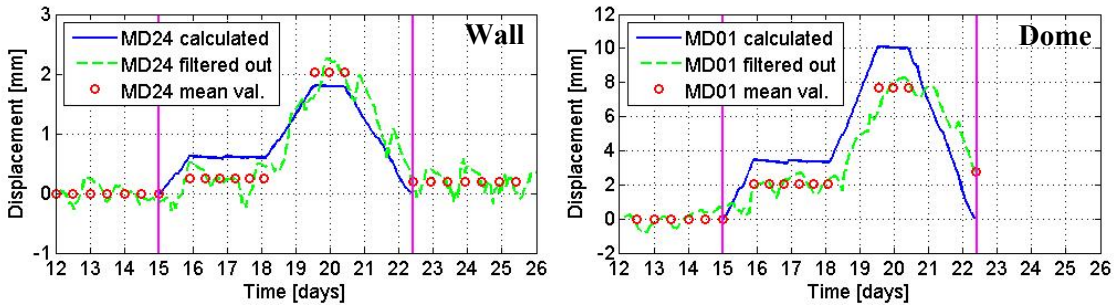

Figure 8. Displacements due only to internal pressure.

Figure 9 shows the maximum of the absolute values of calculated displacement by pressure (left) and temperature (right) during the 29.4 days considered in the numerical simulation, where it can be seen that values due to temperature are approximately half of those due to pressure. Figure 10 presents the maximum, minimum and average values of displacements due to temperature that occur along each line of records within 24 hours around the maximum absolute displacement of each line. Although maximum values are similar to those shown on the right hand side of Figure 9, the remaining curves show the daily fluctuations in correspondence with the maximum seasonal absolute values. Figure 11 is analogous to the previous one; in this case, it shows the curves associated to a period of almost 24 hours corresponding to the maximum pressure, which does not represent a condition of extreme thermal influence as observed for the previous case. The maximum displacements that occur at moments of maximum pressure reach 0.5 mm, which is a significant amplitude respect to the values produced by the pressurization.

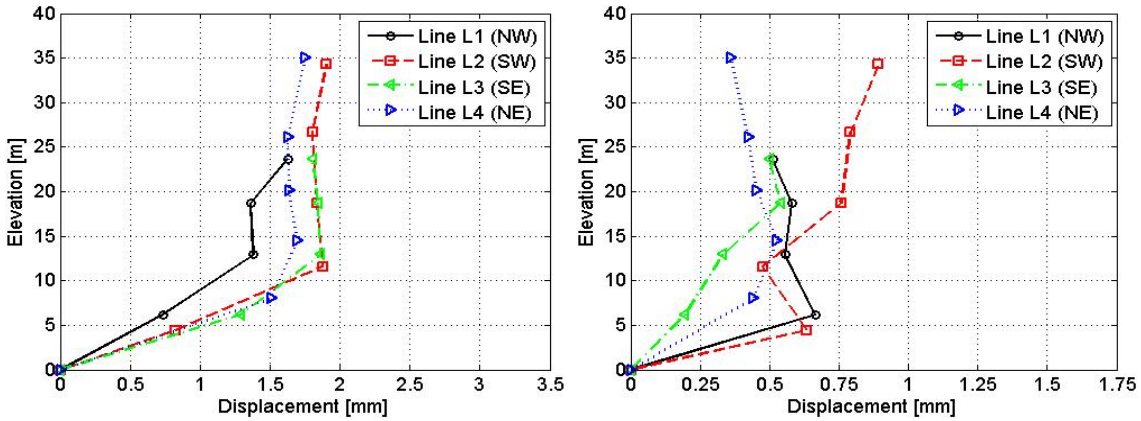

Figure 9. Maximum absolute values of calculated displacement by pressure (left) and temperature (right).

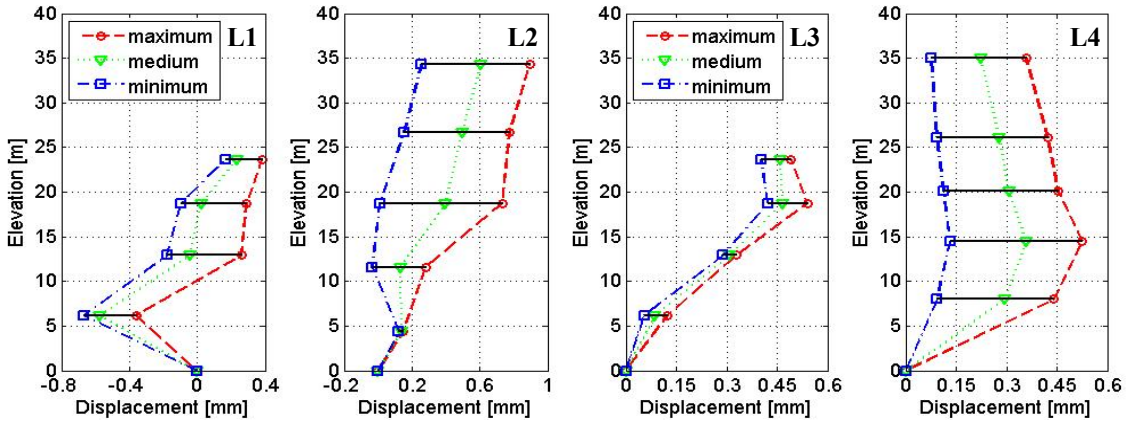

Figure 10. Displacements due to temperature in 24 hours around the maximum displacement per line.

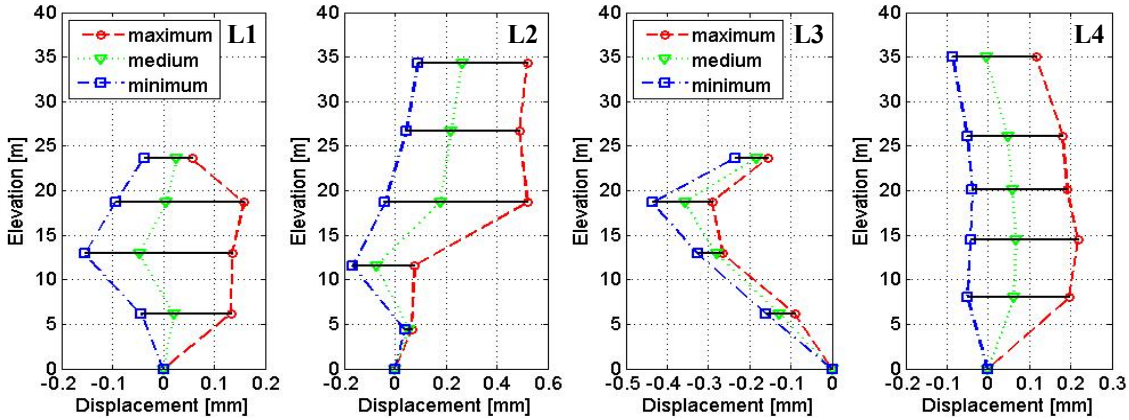

Figure 11. Displacements due to temperature at maximum pressure.

4 CONCLUSIONS

Once the deformations due to the thermal variations were filtered out, results show that the displacements at the maximum applied pressure were in good agreement with the expected values, thus evidencing essentially linear elastic behavior for the maximum pressure attained during the test. As a side note, it is observed that the performance of the structure during the testing after more than 30 years of service is in remarkable agreement with the reported behavior during the initial pressure test carried out in 1981 before the plant went in operation.

5 REFERENCES

Abaqus Finite Element Software v6.10, 2010, *Dassault Systèmes Simulia Corp.*, Providence, RI, USA.

Ceballos, M.A., Estrada, C.F., Pinto, F., Barrera, A. and Prato, C.A., 2019, Evaluation of the Structural Response of the Containment Structure of a NPP to Internal Pressure and Thermal Gradients, *submitted to 25º Conference on Structural Mechanics in Reactor Technology (SMiRT 2019)*, Charlotte, NC, USA.

Ceballos, M.A., Pinto, F., Rocca, R.J. and Prato, C.A., 2007, Seismic Analysis of Embalse Nuclear Power Plant for Life Extension Assessment, *19º Conference on Structural Mechanics in Reactor Technology (SMiRT 19)*, Toronto, Canada, Paper # K16/3.

Pinto, F., Ceballos, M.A., Rocca, R.J. and Prato, C.A., 2007, Validation of Numerical Model of Embalse Nuclear Power Plant Based on Free Field and In-House Records of a Seismic Event, *19º Conference on Structural Mechanics in Reactor Technology (SMiRT 19)*, Toronto, Canada, Paper # K07/4.